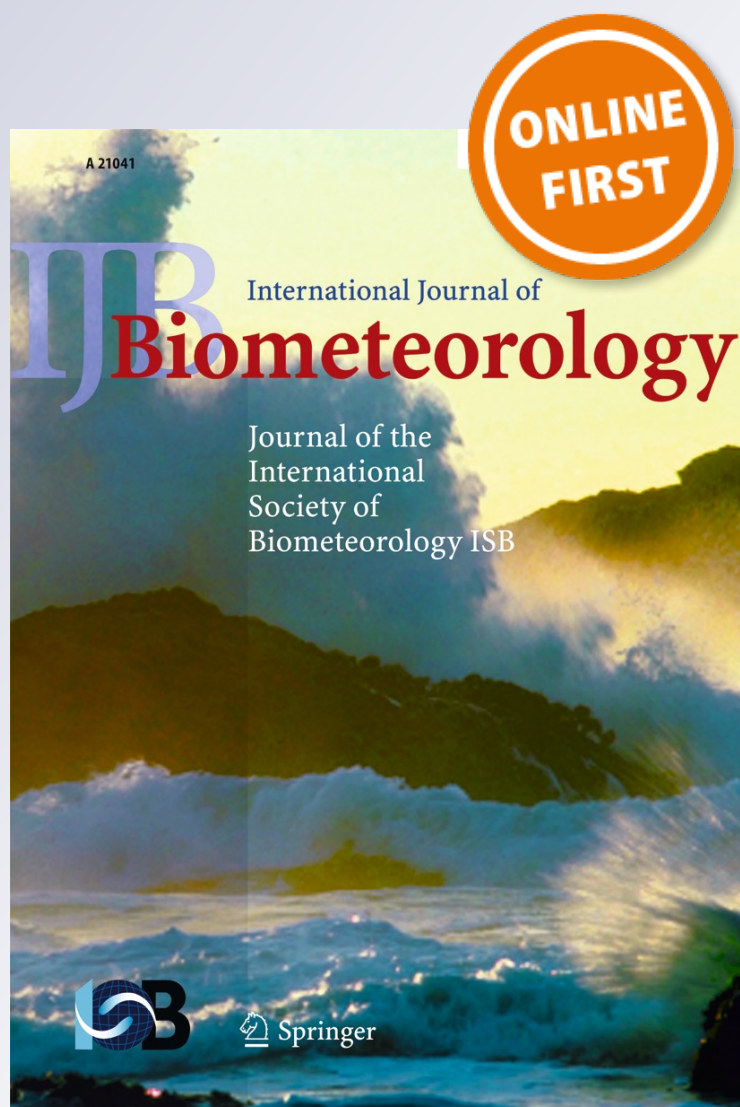# Comparing land surface phenology derived from satellite and GPS network microwave remote sensing

Matthew O. Jones, John S. Kimball, Eric E. Small & Kristine M. Larson

A 21041

International Journal of

Biometeorology

Journal of the
International
Society of
Biometeorology ISB

ISB

 Springer

 Springer

Springer

ORIGINAL PAPER

Comparing land surface phenology derived from satellite and GPS network microwave remote sensing

Matthew O. Jones · John S. Kimball · Eric E. Small · Kristine M. Larson

Abstract The land surface phenology (LSP) start of season (SOS) metric signals the seasonal onset of vegetation activity, including canopy growth and associated increases in land-atmosphere water, energy and carbon (CO_2) exchanges influencing weather and climate variability. The vegetation optical depth (VOD) parameter determined from satellite passive microwave remote sensing provides for global LSP monitoring that is sensitive to changes in vegetation canopy water content and biomass, and insensitive to atmosphere and solar illumination constraints. Direct field measures of canopy water content and biomass changes desired for LSP validation are generally lacking due to the prohibitive costs of maintaining regional monitoring networks. Alternatively, a normalized microwave reflectance index (NMRI) derived from GPS base station measurements is sensitive to daily vegetation water content changes and may provide for effective microwave LSP validation. We compared multiyear (2007–2011) NMRI and satellite VOD records at over 300 GPS sites in North America, and their derived SOS metrics for a subset of 24 homogenous land cover sites to investigate VOD and NMRI correspondence, and potential NMRI utility for LSP validation. Significant correlations ($P < 0.05$) were found at 276 of 305 sites (90.5 %), with generally favorable correspondence in the resulting SOS metrics ($r^2 = 0.73$, $P < 0.001$, RMSE = 36.8 days). This study is the first attempt to compare satellite microwave LSP metrics to a GPS network derived reflectance index and highlights both the utility and limitations of the NMRI data for LSP validation, including spatial scale discrepancies between local NMRI measurements and relatively coarse satellite VOD retrievals.

Introduction

Temporal variation in the seasonal onset of vegetation growth due to climate change has been documented across multiple scales from in situ measures of species-specific first leaf and first flower events (Wolfe et al. 2005) to continental and global scale assessments of canopy leaf onset (Zhang et al. 2007) and growing season length (Piao et al. 2007). Accurate measures of major land surface phenology (LSP) events such as the start, peak and end of the growing season are critical for land-atmosphere, water, energy, and carbon modeling applications (Peñuelas et al. 2009; Morisette et al. 2009). For over 30 years, satellite remote sensing derived vegetation indices, including the normalized difference vegetation index (NDVI) from optical-infrared (IR) sensors, have provided direct LSP measures of the phenological state of vegetation from landscape to global scales (Tarpley et al. 1984; Running and Nemani 1988). Global LSP monitoring from satellite optical-IR remote sensing is constrained over many areas by clouds and

M. O. Jones (✉) · J. S. Kimball
Flathead Lake Biological Station (FLBS), Numerical Terradynamic Simulation Group (NTSG), University of Montana, Davidson Honors College Room 021, NTSG Annex, 32 Campus Dr., Missoula, MT 59812, USA
e-mail: matt.jones@ntsg.umt.edu
URL: http://www.umt.edu/flbs/people/Jones~3409

M. O. Jones · J. S. Kimball
Numerical Terradynamic Simulation Group, The University of Montana, Missoula, MT 59812, USA

E. E. Small
Department of Geological Sciences, The University of Colorado, Boulder, CO 80309, USA

K. M. Larson
Department of Aerospace Engineering Sciences, The University of Colorado, Boulder, CO 80309, USA

Springer

atmosphere aerosol contamination, and seasonal reductions in solar illumination at higher latitudes; this degrades the temporal fidelity of the resulting vegetation indices, often resulting in high-quality data only available at relatively coarse (e.g., 16-day) intervals. Precision in the resulting LSP metrics, including the vegetation start of season (SOS) is also degraded. Satellite active and passive microwave remote sensing has also been used effectively for global LSP assessments (Kimball et al. 2004; Frolking et al. 2006; Jones et al. 2011). Unlike optical-IR sensors, microwave remote sensing is relatively insensitive to atmosphere and solar illumination constraints, while lower frequency (i.e. ~$\leq$37 GHz) global observations available from existing satellite microwave sensors are sensitive to vegetation water content, canopy structure and biomass changes (Ulaby et al. 1981).

The microwave vegetation optical depth (VOD) parameter defines the frequency dependent extinction of land surface microwave emissions by the intervening vegetation layer (Jackson and Schmugge 1991; Van De Griend et al. 2004) and is related to changes in vegetation water content and biomass. A consistent global VOD record was developed from 18.7, 10.7 and 6.9 GHz frequency brightness temperature (T_b) measurements from the AMSR-E (advanced microwave scanning radiometer for EOS) sensor on the NASA Aqua satellite and provides global coverage and near daily VOD temporal fidelity under classified non-frozen conditions from 2002 to 2011 (Jones and Kimball 2011). These data have been used to demonstrate VOD sensitivity to vegetation canopy changes indicated by satellite optical-IR remote sensing based vegetation indices, including NDVI, Enhanced Vegetation Index, Leaf Area Index and an independent bioclimatic growing season index (Jones et al. 2011). Global VOD variability also followed regional gradients in climate, land cover and canopy biomass, with characteristic seasonal variability observed for the major land cover classes and little evidence of signal saturation at higher canopy biomass levels. The vegetation SOS over North America was determined from the VOD record and followed general ecoregion patterns responsive to climate constraints on vegetation productivity, and proportions of woody vegetation cover. The VOD SOS metrics also corresponded well with site level vegetation SOS estimates derived from flux tower CO_2 eddy covariance measures of gross primary productivity ($r^2=0.61$, $P<0.01$) and ecosystem respiration ($r^2=0.44$, $P<0.01$) at 23 sites across North America (Jones et al. 2012). While the optical-IR and flux tower data provide LSP metrics associated with vegetation canopy greenness and gas exchange, more direct field measurements and validation methods are needed to document changes in canopy water content and biomass.

The relatively common use of satellite optical-IR remote sensing for vegetation studies has allowed for extensive development of validation protocols based on these data, including recent efforts by the Committee on Earth Observation Satellites Land Product Validation (CEOS-LPV) subgroup. These protocols generally involve the use of coordinated in situ measurements including tower-mounted radiometers and long-term field data collections. Other regional efforts are underway to validate satellite optical-IR based LSP metrics using stand level phenology cameras (e.g., the PhenoCam Network, Richardson et al. 2009) and more extensive citizen science based data collections including the USA National Phenology Network (USA-NPN) (Schwartz et al. 2012). Optical-IR vegetation indices are sensitive to canopy greenness, or chlorophyll content, and have the advantage of being directly comparable to easily observed changes in the state of vegetation such as bud burst, leaf unfolding or changes in leaf color. Direct measurements of related changes in canopy water content and biomass structure suitable for satellite microwave VOD and LSP validation require more labor-intensive field measurements. Site level microwave measurements have been made by microwave radiometers, but these data are of limited scope in both space and time, and the focus of such efforts has been primarily to validate satellite soil moisture measures and not the state of vegetation through time or across a range of vegetation types. Few field level microwave datasets are currently available, which has limited the application of these data for satellite VOD and LSP validation. Recent studies however, have revealed that permanent Global Positioning System (GPS) stations installed to measure tectonic plate motions, can be used to detect ecosystem relevant biophysical parameters, including surface soil moisture (Larson et al. 2008) and vegetation water content variability (Small et al. 2010). GPS satellites transmit L-band (1.2 and 1.5 GHz frequency) microwave signals. These signals interact strongly with water in the environment (including vegetation), and thus are suitable for monitoring temporal variations in biophysical parameters. GPS stations are designed for determining spatial location. They measure the distance between the local station antenna and the orbital constellation of GPS satellites. A secondary signal, and noise source for positioning applications, measures signal reflectance within a local footprint of approximately 1,000 m^2 (~0.001 km^2) surrounding the GPS antenna. The NMRI (normalized microwave reflection index) metric is derived from these GPS reflections; it can be measured on a daily basis and is insensitive to cloud cover (Larson and Small 2013). This study uses an initial compilation of NMRI records from GPS sites distributed across the western United States.

The objective of this investigation was to quantify spatial and temporal correspondence between satellite (AMSR-E) derived VOD and in situ NMRI network observations to assess the potential of the NMRI data for satellite microwave LSP validation. We compared vegetation water content changes inferred from GPS NMRI site network data with collocated satellite VOD records over the western continental USA and Alaska. The NMRI and VOD observations were

compared at 305 GPS site locations over a multi-year observation record from January 2007 to September 2011. The NMRI and VOD time series were processed to determine the vegetation SOS for a subset of 24 GPS sites determined to have regionally homogeneous land cover conditions within the overlying (25 km resolution) VOD grid cell; the resulting SOS metrics were then compared to evaluate NMRI and VOD consistency in determining this critical LSP metric. Spatial heterogeneity of LSP, which potentially could affect VOD and NMRI correspondence, was examined for a single AMSR-E VOD grid cell containing multiple NMRI sites; for this location, the VOD record was evaluated against NMRI observations from nine GPS antennas and 250 m resolution satellite (MODIS) NDVI records representing different land cover types within the overlying VOD grid cell to analyze the effect of mixed land cover contributions on the aggregate regional SOS metric.

Data and methods

Microwave vegetation optical depth

The Advanced Microwave Scanning Radiometer for EOS (AMSR-E) is deployed on the polar-orbiting Aqua satellite platform with UTC 1:30 a.m. (descending)/p.m. (ascending) orbit equatorial crossings. The AMSR-E sensor measures vertical and horizontal polarized brightness temperatures at six frequencies (6.9, 10.7, 18.7, 23.8, 36.5, 89.0 GHz), and at a constant Earth incidence angle of 55° from nadir. The daily 25 km resolution global equal area scalable Earth (EASE) Grid brightness temperatures provided by the NASA data archive facility at the National Snow and Ice Data Center (Knowles et al. 2009) were used to derive an AMSR-E global land parameter database for ecosystem studies (Jones and Kimball 2011). The database includes VOD retrievals at 6.9, 10.7 and 18.7 GHz frequencies; the VOD series derived from the 18.7 GHz T_b record was employed for this investigation due to greater radio frequency interference (RFI) and associated retrieval gaps in the 6.9 and 10.7 GHz frequency data (Njoku and Ashcroft 2005). The VOD record extends from January 2003 to September 2011 and encompasses all grid cells with <50 % permanent ice or open water cover, as defined from a 1 km resolution MODIS (MOD12Q1) IGBP global land cover classification aggregated to 25 km resolution, while retaining relative land cover class proportions (Knowles 2004). The VOD retrieval algorithms minimize potential noise effects from dynamic atmosphere precipitable water vapor, temperature, surface inundation and soil moisture, resulting in global consistency and relatively high accuracy (Jones et al. 2009). A detailed description of the AMSR-E VOD record, including algorithm development and sensitivity, is provided elsewhere (Jones et al. 2009, 2011).

In this study the daily VOD record from January 2007 to September 2011 was temporally composited to a 4-day median time step. This compositing mitigates signal noise and allows for the creation of a continuous time series, overcoming missing data due to observation swath coverage gaps from the polar orbiting AMSR-E sensor at mid- to lower latitudes. At higher latitudes without gaps the 4-day median is defined as the larger of the two middle values.

GPS normalized microwave reflection index

The GPS is a constellation of over 30 L-band (1.5 and 1.2 GHz) transmitting satellites that is best known for real-time navigation and positioning applications. Earth scientists have exploited GPS signals to measure slow tectonic variations (mm/year) by installing and maintaining regional base station networks that operate continuously. Recently the National Science Foundation installed over 1,000 GPS base stations in the western United States to measure deformation of the Pacific-North America plate boundary as part of the EarthScope Plate Boundary Observatory (PBO) initiative (http://www.earthscope.org). Most sites were installed by 2007 and operate with nearly identical instrumentation (receivers and antennas). GPS sites are generally located in low vegetation biomass areas to minimize off nadir reflectance contamination of the GPS signal. The resulting NMRI (Small et al. 2010) site records reflect largely grassland and shrubland conditions with limited coverage of higher biomass (e.g., forest) vegetation types (graph in Fig. 1).

The NMRI vegetation metric is based on reflected GPS signals (multipath) observed in the L1 GPS ranging data, or MP1 (MultiPath on the L1 frequency) from the PBO network. The reflections are quantified by calculating the mean of the daily observation scatter (RMS) for all satellites, or MP1rms (Estey and Meertens 1999). While the MP1rms statistics are calculated routinely by GPS base station networks, GPS station operators use them primarily to evaluate hardware performance. Small et al. (2010) were the first to show that these variations in MP1rms are correlated strongly with the NDVI ($0.60 < r^2 < 0.80$) in the western US (Idaho, Colorado, Montana, Utah, Nevada, Oregon). The GPS base station sites examined represented a range of land cover types, including grassland, cropland and shrubland. Amplitudes of the reflected signals are strongest when vegetation biomass within the local (~0.001 km²) sampling footprint is relatively low, and decrease as vegetation biomass and associated water content increases. The RMS of the observation scatter captures these reflection amplitude variations.

Building on that initial study, the PBO H₂O group has compiled normalized MP1rms statistics (NMRI) for more than 300 GPS stations from the PBO network and extended it in time to 2012 (http://xenon.colorado.edu/portal). The data are screened for snow presence and recent precipitation as
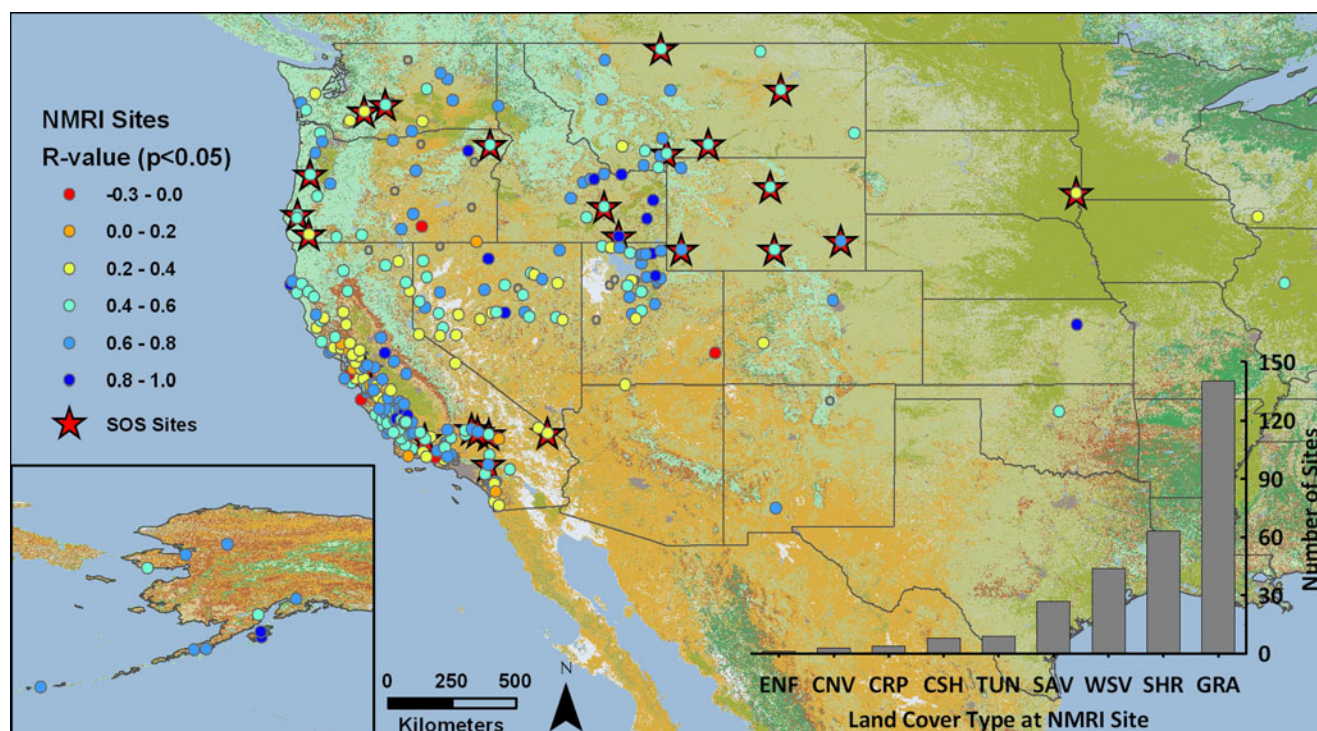
Fig. 1 Pearson correlation coefficients ($P<0.05$) between vegetation optical depth (VOD) and normalized microwave reflectance index (NMRI) time series for 305 GPS base station sites across the western US. *Inset* Sites over the Alaska portion of the domain. *Open circles* Non-significant ($P>0.05$) correlation sites, *stars* 24 homogeneous land cover sites used in the start of season (SOS) calculations. *Graph* Number of NMRI sites by land cover type as designated by the Plate Boundary Observatory (PBO) network (*ENF* evergreen needle leaf forest, *CNV* cropland/natural vegetation mosaic, *CRP* cropland, *TUN* tundra, *SAV* savanna, *WSV* woody savanna, *SHR* shrubland, *GRA* grassland). Background represents the MODIS IGBP land cover classification

these adversely affect the signal and resulting NMRI value. Because reflected GPS signals are also influenced by terrain (a reflected GPS range signal depends directly on the extra path length), the MP1rms metrics have been normalized to remove this first-order effect. The bare vegetation state is determined empirically by estimating the maximum MP1rms over the entire observation record (MP1max). Dividing the variation in MP1rms by this maximum removes the extra path length term. The NMRI thus measures variation in the GPS microwave (L-band) reflection power:

$$NMRI = -(MP1rms–MP1max)/MP1max \qquad (1)$$

The negative sign in Eq. (1) is introduced to allow the NMRI to increase or decrease as vegetation grows or senesces. Further information on the NMRI database and validation with field measurements is available from Larson and Small (2013) and Small et al. (2013). In this study NMRI data from January, 2007 to December, 2011 for 305 sites within the western continental United States and Alaska were composited to the same 4-day median time step as the VOD to allow for direct comparison and to minimize potential effects from day-to-day variability on the phenology signal.

Correlations and phenology metrics

Pearson correlation coefficients and significance values were calculated between 305 NMRI 4-day time series and corresponding VOD 25 km resolution grid cell time series for the full data record and for each calendar year. Full data record lagged correlations were also evaluated between the VOD and NMRI series by systematically offsetting the VOD series by up to $+/-$ 48 days (12 4-day time steps). To assess the influence of land cover heterogeneity on the NMRI and VOD correlations, full data record R-values for each NMRI location were compared to a land cover heterogeneity index [Shannon diversity index (SDI)] (Shannon 1948), MODIS derived percent tree cover (Hansen et al. 2003) and terrain heterogeneity (SD of elevation) within the overlying 25 km VOD grid cell.

NMRI sites that contained the full 5-year data record and were within homogeneous VOD grid cells (>80 % common land cover) were selected for SOS phenology metric calculations; this resulted in 24 sites well distributed across the western US (Fig. 1). The homogeneous VOD grid cells were identified using the 1 km resolution MODIS (MOD12Q1) IGBP global land cover classification (Knowles 2004). Many of the 24 homogeneous land cover sites are located in regions where winter snow cover is common. The NMRI and

VOD temporal series are degraded and screened during these periods, resulting in winter gaps in the data records that must be filled in order to apply fitting algorithms and calculate LSP metrics. Winter gaps were filled on a site or grid cell-wise basis for each year using the median of the first three NMRI or VOD values of the following spring. This approach assumes that vegetation will degrade or reach a minimum stasis and remain relatively constant (dormant) through the frozen winter period, and that the first successful retrievals of the following spring effectively represent the winter base vegetation state.

The 4-day median filled NMRI and VOD time series were input into TIMESAT (Jönsson and Eklundh 2004), a commonly used tool for analyzing time series data (Nightingale et al. 2009; Tan et al. 2011) that provides curve fitting methods for defining phenology metrics and allows for the detection of dual (biannual) seasons. A double logistic fit was applied to the time series data and the SOS was defined as the 20 % threshold of seasonal amplitude. TIMESAT requires previous and subsequent season data to classify the current (middle) season SOS metric. Therefore, the 5 year (2007–2011) NMRI and VOD records produced 3 to 4 annual (or 6 to 8 biannual) SOS metrics per site. Linear regression analysis and root mean squared error (RMSE), mean absolute error (MAE), and mean residual error (MRE) statistics were then used to compare the NMRI and VOD SOS metrics.

NMRI and VOD sensitivity to moisture variability

As the NMRI and VOD are responsive to changes in vegetation water content, climatic variations (in particular those associated with water availability), at the local and regional scale may affect seasonal and interannual variation in both data records, and their correspondence. To assess these effects, NMRI and VOD correlations for each calendar year were compared to a yearly Palmer drought severity index (PDSI) (Palmer 1965; Dai et al. 2004) and the number of precipitation days per year (Harris et al. 2013) within the VOD 25-km footprint for each site. Variation in the two data records was further assessed in relation to monthly changes in the atmosphere vapor pressure deficit (VPD).

The VPD term is a measure of the evaporative demand of the atmosphere and has been shown to be an effective indicator of water limitation to vegetation growth (Huffaker 1942). High VPD values are representative of water stress and, if consistent over time, can significantly limit photosynthesis and growth (White et al. 2000). The NMRI and VOD time series were composited to 16-day intervals and temporal anomalies were calculated for each data record in relation to their long-term means. These results were then plotted in relation to corresponding 0.5° resolution monthly VPD anomalies derived from the NASA MERRA (Modern-Era Retrospective Analysis for Research and Application) global

reanalysis daily surface meteorology (Rienecker et al. 2011). Anomalies (X_i*) were calculated as

$$X_i* = X_i - \mu X_i \qquad (2)$$

where X_i is the 16-day (NMRI, VOD) or monthly (VPD) value and μX_i is the mean 16-day or monthly value for all years (2007–2011). The standard deviation of the anomalies was calculated for the NMRI and VOD, and 16-day anomalies were considered significant departures from normal if they positively or negatively exceeded one standard deviation. The 16-day intervals were then flagged if NMRI and VOD anomalies were both positive or negative departures from normal.

Multiple sites within a single VOD grid cell

As the NMRI is calculated at over 300 GPS base stations in the western US, there are multiple VOD grid cells containing more than one NMRI site. The AMSR-E 25 km resolution VOD retrievals often represent a mix of underlying land cover types and environmental conditions, especially over complex terrain, while the NMRI represents a finer scale (~0.001 km^2) footprint surrounding the GPS antenna and often represents a single land cover type. To evaluate potential effects of NMRI heterogeneity, the VOD grid cell with the most NMRI sites (nine) was identified. The selected VOD grid cell area also contained a mix of herbaceous and woody biomass components; 53 % grassland, 32 % shrubland, and 12 % woody savanna. The grid cell (center coordinates: latitude 35.7544°, longitude −120.2603°) is located in south-central California and encompasses a topographic range from ~300 to 700 m with an approximate mean annual temperature of 18.3 °C and mean annual precipitation of 21.0 cm. The initiation of vegetation growth in this relatively warm region is driven by fall or early winter (October–January) precipitation onset. Daily precipitation data (Klein Tank et al. 2002) were acquired from the National Climate Data Center for the Coalinga, California station (GHCND:USC00041864), approximately 28 km north of the VOD grid cell. As recent precipitation and soil moisture variation adversely affect the NMRI values, days with precipitation (and the following day) were further screened using the local precipitation data. Eight of the nine NMRI sites are located in grassland and the remaining site in shrubland (note: data availability began in 2008 for sites p542, p552 and p578). We compared the single VOD time series to the nine NMRI time series and MODIS NDVI (MOD13Q1) 250 m time series spatial means of the three dominant land cover types and overall NDVI spatial means within the overlying VOD grid cell. The SOS metrics were calculated using the double logistic fit and 20 % of seasonal amplitude in TIMESAT for all time series.

Results

VOD and NMRI correlations

Pearson correlation coefficients between 4-day VOD and NMRI time series at the 305 GPS site locations are displayed in Fig. 1. Of the 305 sites, 276 (90.5 %) showed significant ($P<0.05$) positive correlations between the VOD and NMRI time series, while 12 sites displayed negative correlations, five of which were significant ($P<0.05$). The mean of significant correlation coefficients was $R=0.53$ (SD=0.21). Using temporally lagged VOD series improved the VOD-NMRI correlations at 250 sites, improving the mean of significant correlation coefficients; $R=0.61$ (SD=0.17). The non-lagged and lagged correlation results, grouped by local NMRI land cover type, are summarized in Fig. 2. A majority (75 %) of sites achieved the best correspondence with a VOD lag from −4 to 32 days relative to the NMRI (Fig. 2, inset); a positive (negative) lag implies that the VOD season onset begins earlier (later) than the NMRI season onset.

The VOD and NMRI correlations were highly variable within land cover types (Fig. 2) and examination of the individual calendar year correlations revealed a logistic relationship between each site's coefficient of variation (CV) and its mean R-value for all 4 years of record; sites with lower R-values generally displayed a higher CV. Although some site years displayed strong correlations, other site years showed weak correspondence, adversely affecting the full data record R-values shown in Fig. 2. No significant relationships were found between VOD and NMRI correspondence for the full-data record and terrain heterogeneity (SD of elevation), MODIS percent tree cover or land cover heterogeneity (SDI).
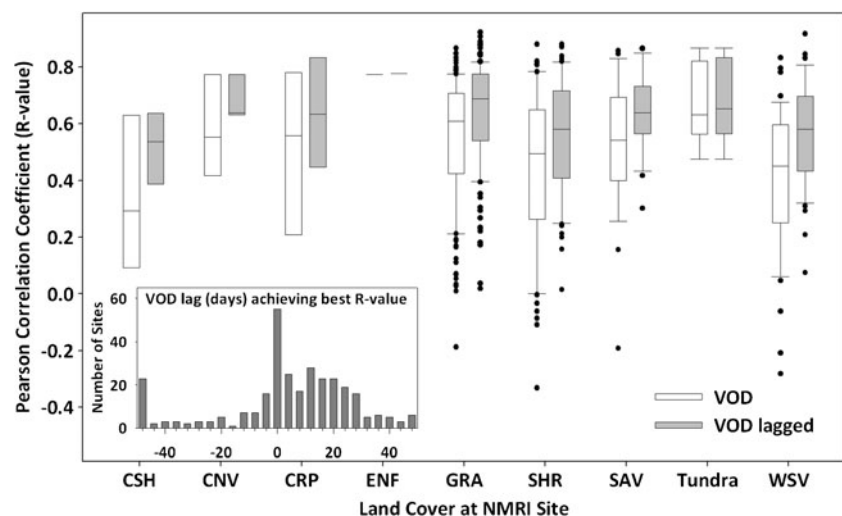
The NMRI and VOD 16-day anomalies displayed widespread favorable agreement in their departures from normal across a large latitudinal range (32.6° N to 67.0° N) that were generally congruent with monthly VPD anomalies (Fig. 3). High VPD anomalies were observed across the full latitudinal range in 2007 and both the NMRI and VOD displayed coincident negative anomalies at a majority of the sites. The opposite response is seen in years 2010 and 2011, with lower than normal VPD and higher than normal NMRI and VOD, particularly at more southerly latitudes of the western US domain where water availability is a primary control on vegetation activity. Despite this favorable agreement with VPD, no significant relationship was found between the degree of VOD and NMRI correspondence and yearly PDSI or precipitation days per year.

Start of season metrics

A linear regression of the VOD versus NMRI derived SOS (day of year) values for the 24 homogenous land cover sites resulted in a coefficient of determination (r^2) of 0.73 ($P<0.001$), RMSE of 36.8 days and MAE of 26.7 days (Fig. 4). The MRE in SOS values (VOD SOS – NMRI SOS) was −36.2 days for all sites with 95 % of VOD seasons starting earlier than NMRI seasons. In some cases the SOS begins near the end of a calendar year for one dataset (e.g., day of year = 355, year = 2009) and at the beginning of the calendar year for the second dataset (e.g., day of year = 20, year = 2010). In order to properly plot these values and perform a linear regression analysis, the day of year values must be adjusted. For the example given, the 2009 SOS is classified as a 2010 SOS and adjusted to day of year −10 to properly account for the 30 day difference; this accounts for the negative day of year values in Fig. 3. Eight sites displayed one or more seasons with differences greater than 60 days and a single site displayed a consistent offset greater than 90 days (Fig. 3, open symbols). Full data record correlation coefficients at these sites ranged from 0.21 to 0.81, indicating that the local NMRI response for some sites may not be representative of the homogeneous land cover

Fig. 2 VOD versus NMRI correlations and temporally lagged correlations, grouped by land cover type at the individual NMRI sites. Plot displays median, quartiles, 5th and 95th percentiles and outliers. *Inset* Number of sites that achieved their highest correlation coefficient at the given temporal lag
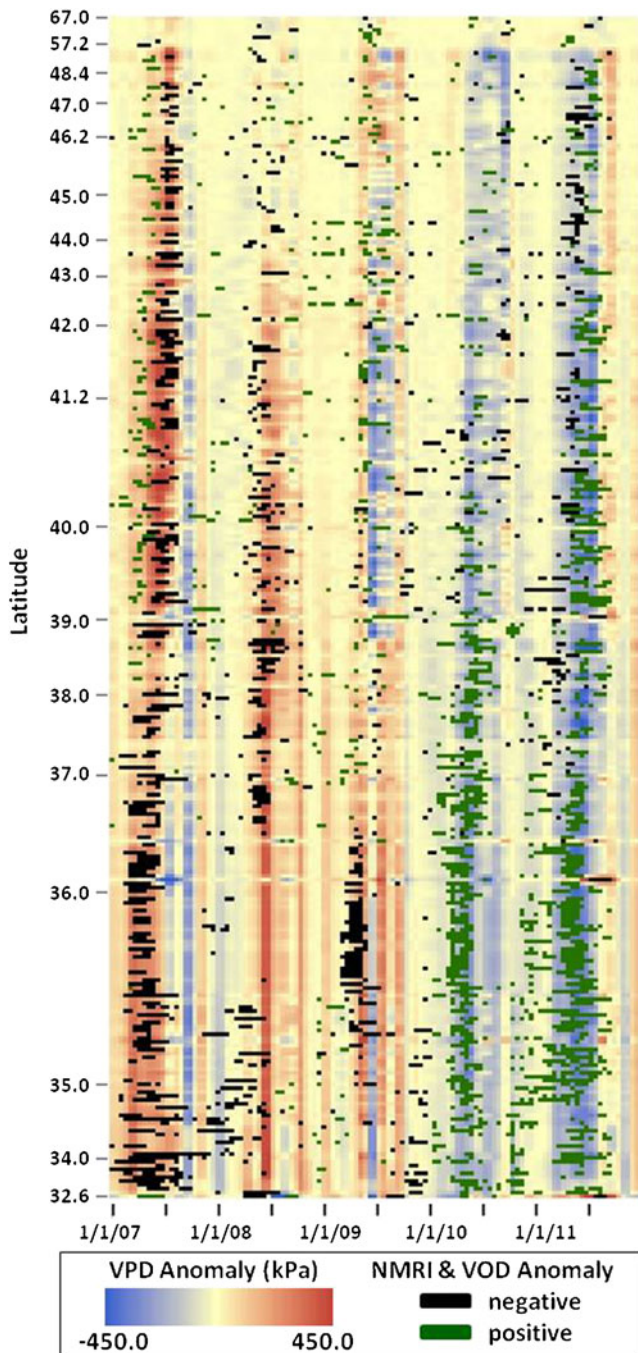
Fig. 4 Least-squares linear regression fit between VOD and NMRI derived SOS values at the 24 homogeneous land cover sites for the 2007–2011 record. Mean absolute error (MAE) = 26.7 days. Each NMRI site is given a unique symbol

cover heterogeneity (SDI). A lower SDI represents low variability in land cover and therefore an inverse relationship is expected; pixels with low SDI values are expected to have stronger NMRI-VOD correlations, but this relationship was not apparent in the analysis. Examination of multiple NMRI sites within a single VOD grid cell partially explains these discrepancies.

NMRI and NDVI heterogeneity within a single VOD grid cell

The mean and standard deviation of the nine NMRI site records located within the single VOD grid cell are plotted in Fig. 5a along with the VOD time series and overall NDVI mean of the three dominant land cover classes, which comprise 97 % of the overlying VOD grid cell. These results display a fall (~September) VOD increase that then decreases with winter onset (December–January) in 2008 and 2010, but is relatively stable through the other winters of record (2009, 2011). The mean NDVI time series of each dominant land cover class (Fig. 4b) within the VOD cell displays a response in the fall of some years similar to the VOD record, particularly for woody savanna. There is good agreement ($0.40 < R < 0.82$, $P < 0.01$) between all of the time series displayed in Fig. 4, including similar interannual variation in seasonal amplitudes, with years 2008, 2010 and 2011 all displaying high amplitudes and 2007 and 2009 displaying lower than normal amplitudes for the record.

The SOS metrics for all of the time series, including individual metrics for each NMRI site and seasonal precipitation accumulation from 1 July to 30 June, are displayed in Fig. 6a. These results demonstrate the wide variation that can occur in calculating phenology metrics even though the time series are relatively similar. The SOS values for the NMRI sites occur within approximately 1 month except for a single site (p542) in 2010–2011 and the drought year (2008–2009) when two of the five available sites displayed no SOS and the remaining sites displayed a SOS range of 113 days; an effect of the

Fig. 3 Space (*y*-axis) vs time (*x*-axis) plot of NMRI and VOD 16-day anomalies (2007–2011) determined as significant departures from normal and plotted over monthly vapor pressure deficit (VPD) anomalies at each of the 305 NMRI sites. Each site is represented by a row of pixels distributed along the time (*x*) axis, while sites are ordered by latitude along the *y*-axis. *Green* and *black* pixels represent 16-day intervals when both NMRI and VOD anomalies were significantly positive or negative departures from normal; i.e., greater than or less than the SD of the full data record anomalies

conditions of the larger (25-km resolution) VOD grid cell, resulting in a large offset in the associated SOS metrics. This is also apparent in the lack of significant correspondence between the VOD and NMRI time series correlations, and land
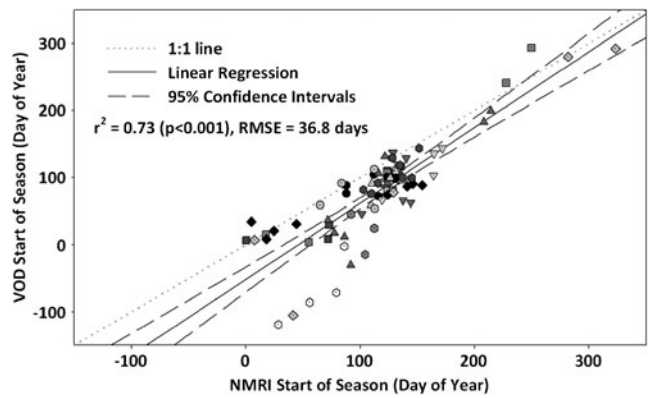
Fig. 5 **a** The spatial mean and standard deviation of 4-day median time series from nine NMRI sites located within a single VOD grid cell, the mean 16-day 250 m MODIS (MOD13Q1) NDVI of the three dominant land cover types within the VOD grid cell, and the corresponding VOD time series. The nine NMRI sites represent grassland (eight sites) and shrubland (one site) conditions; **b** the mean NDVI time series from individual dominant land cover classes representing 53 % (GRA), 32 % (SHR), and 12 % (WSV) of the overlying VOD grid cell
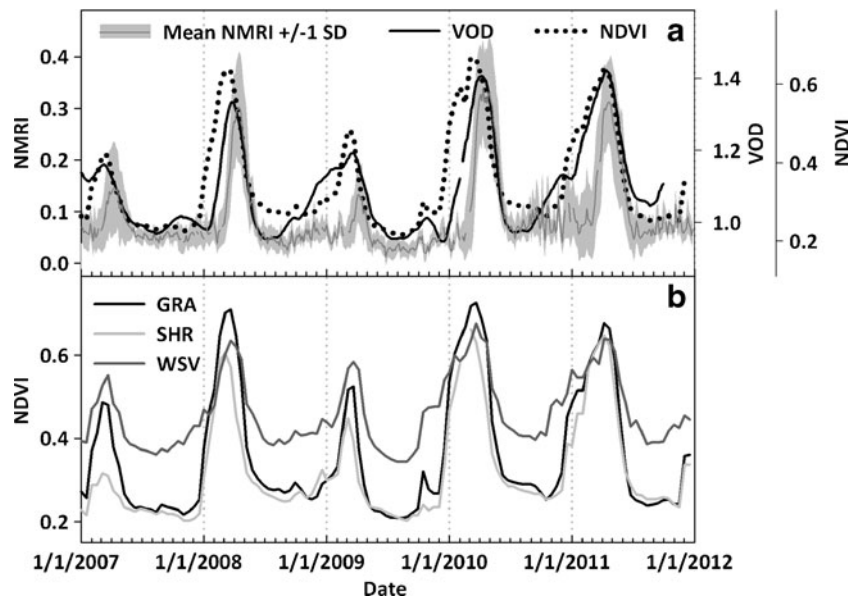
minimal variation in NMRI values for that season (Fig. 4a). The VOD SOS displays large interannual variation, which is dependent on whether a winter (November–January) VOD trough is present following the initial VOD rise in September.

Full data record correlations between the NMRI series for the individual sites and the overlying grid cell VOD time series ranged from 0.56 to 0.87 (P<0.01 all cases). Three sites (p539, p542, p552) with high correlations (R=0.87, 0.83 and 0.76, respectively) displayed increasing NMRI values in the fall (September–December) of years 2008 and 2011, similar to the VOD record (Fig. 6b). These three sites are located within 10 km of each other in the southern portion of the VOD

grid cell and at the highest elevations (>600 m) within the cell; elevations at the nine sites ranged from 384 to 612 m. Although the fall NMRI increases at these sites were not significant enough to trigger a SOS designation, except for the 2010 SOS for p542, they appear to be the best representation of the pixel-wide VOD signal.

Discussion

The large number of significant temporal correlations (276 of 305 sites) between the satellite derived VOD and in situ

Fig. 6 **a** TIMESAT estimated SOS (day of year) for the 2007–2011 record derived for the nine NMRI sites, and MODIS NDVI and VOD time series within the single VOD grid cell; cumulative daily precipitation from a nearby weather station is also shown (*grey bar*); the NMRI site SOS values are labeled by PBO Site ID, and NDVI based SOS values by their respective dominant land cover classes (GRA, SHR, WSV) and the overall NDVI mean (Mean). The lower graphic **b** shows the VOD time series and three representative land cover NMRI site time series (p539, SHR; p542 and p552, GRA) within the single VOD grid cell
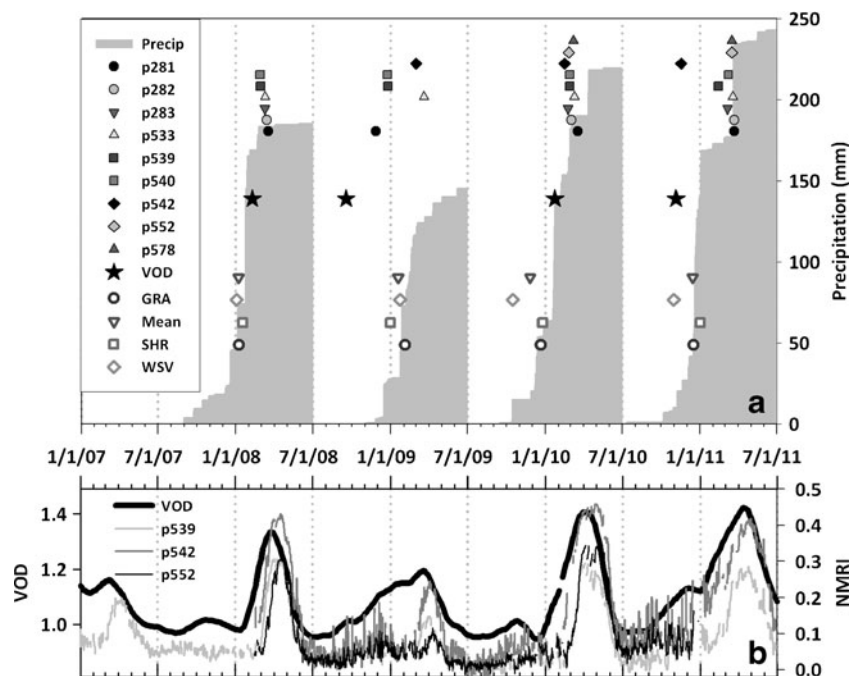
NMRI records indicate broad regional agreement between the two microwave vegetation metrics, despite the large difference in relative footprint size between the ~0.001 km^2 NMRI retrievals and the 625 km^2 VOD grid cells. The sign and magnitude of NMRI and VOD temporal (16-day) anomalies was generally coincident with variability in the monthly VPD used as a surrogate indicator of plant-available moisture controls on vegetation activity; positive (negative) NMRI and VOD anomalies generally coincided with below (above) average VPD levels relative to the long-term record. These results indicate similar climate sensitivity of both vegetation water content metrics despite relative differences in the microwave frequency and spatial scale of the retrievals.

The lagged correlation results indicate that VOD seasonality generally precedes NMRI seasonality by approximately 0 to 30 days. This temporal lag was confirmed by the SOS results at the 24 homogeneous land cover sites and the analysis of sub-grid scale heterogeneity within a single VOD grid cell. The observed spatial heterogeneity and interannual variation of sub-grid NMRI and NDVI time series within the single VOD grid cell help to explain the variation in correlation values within and across land cover categories (Fig. 2) and highlight the difficulty in calculating consistent LSP metrics from datasets measuring different land surface properties, and with large differences in spatial resolution (Figs. 4, 6a). Sites with relatively weak temporal NMRI and VOD correlations for the full data record generally displayed higher variability (CV) in their yearly correlations; this was often a result of 1 or 2 years displaying poor correlations and adversely affecting the full data record R-value for a given site. The VOD grid cell coinciding with multiple NMRI sites used for the land cover heterogeneity analysis is characteristic of this pattern, as one NMRI site displayed a negative NMRI-VOD correlation 1 year ($R=-0.47$) and a strong positive correlation the following year ($R=0.68$, $P<0.01$), while two nearby sites had variable yearly R-values ranging from 0.11 and 0.24 to 0.57 and 0.63, respectively.

Although both the NMRI and VOD showed similar sensitivity to regional VPD changes, other climatic (PDSI, precipitation days per year) and landscape variability (SD of elevation, SDI, percent tree cover) indicators were unable to explain the NMRI-VOD correlation patterns. The observed range of full data record correlation coefficients ($R=0.56$ to 0.87) between the nine NMRI sites and the single VOD grid cell indicate that spatial scale discrepancies between the relatively coarse VOD retrievals and local scale NMRI measurements likely influence the VOD-NMRI correlation patterns and associated SOS metrics.

Large spatial heterogeneity in vegetation phenology may occur within a single vegetation class and may not be effectively represented by a single NMRI site even when located within the regionally dominant land cover class. For example, a subset of the MCD12Q2 500 m MODIS Land Cover Dynamics Product from 2007 to 2010 within this VOD grid cell displays within season greenup dates ranging across ~51 days for grassland areas, ~53 days for shrubland areas, and ~40 days for woody savanna areas. Both herbaceous and woody vegetation components within this single VOD grid cell contribute to the aggregate microwave attenuation. If these vegetation components exhibit variations in seasonal onset, the VOD and NMRI SOS values may display significant variation dependent on which component is the primary contributor to the aggregate VOD signal and where the NMRI site is located within the VOD grid cell. For example, in a field study conducted in a similar mixed grassland and woody savanna system as the VOD multi-site pixel, Ma et al. (2007) found a mean SOS difference of 110 days between a grassland site and woody savanna site located approximately 2 km apart.

The SOS discrepancy between the NMRI and VOD data may also be partially explained by the different microwave frequencies of the two retrievals; the GPS network operates at a lower L-band (1.5 and 1.2 GHz) frequency, while the AMSR-E VOD retrievals used in this study are derived from K-band (18.65 GHz) frequency T_b series. The higher frequency (shorter wavelength) AMSR-E retrievals exhibit greater attenuation and scattering from surface vegetation cover, particularly smaller leaf and branch elements. The VOD is therefore expected to exhibit greater sensitivity to changes in vegetation canopy water content, particularly under lower biomass (e.g., grassland) conditions representative of most NMRI sites; this may account for the generally earlier VOD SOS relative to the NMRI results. The difference between NDVI SOS dates and those of VOD or NMRI can also be explained partially by the difference in sensor wavelengths. Optical-IR remote sensing metrics respond to changes in vegetation greenness, or chlorophyll content, and the timing of greenup may not mirror changes in canopy biomass water content (Guan et al. 2012). A previous study (Jones et al. 2012) demonstrated that VOD LSP metrics can lag satellite optical-IR based LSP metrics in regions where water is a primary constraint on vegetation growth, with the temporal lag increasing with the proportion of woody vegetation cover due to microwave sensitivity to both photosynthetic and non-photosynthetic vegetation components. The difference between optical-IR and microwave LSP metrics can therefore provide critical information on the timing of water uptake and allocation versus the creation of new photosynthetic biomass.

This study is the first intercomparison of satellite microwave phenology metrics and a GPS network derived reflectance index; it highlights both promising initial results and limitations to be addressed in future research. The global extent and current design of GPS base stations provide a comprehensive set of daily stand or patch scale (~0.001 km^2) microwave vegetation measures, but there are large discrepancies between the local NMRI footprint and the regional scale satellite VOD

retrievals that hinder direct comparisons and interpretations for global scale microwave LSP validation. Alternative validation sites designed to overcome these discrepancies are needed in order to advance LSP understanding. To overcome spatial scale differences between local observations and overlying satellite retrievals, and limited landscape representation of the NMRI data, GPS stations spanning a full range of land cover variability within a collection of VOD grid cells could be installed. This design would include sites with raised (or top-of-canopy) GPS antennas to provide a larger sampling footprint approaching the scale of the satellite retrievals and allow for retrieval of the NMRI metric in more densely vegetated areas. Potential LSP validation sites incorporating NMRI measurements can be integrated with current phenology observation networks at relatively low cost. These networks provide potentially synergistic observations including phenology cameras (e.g., the PhenoCam network), targeted phenophase observations (e.g., USA-NPN), tower eddy covariance carbon and water flux measurements (e.g., AmeriFlux), and other supporting biophysical measurements (e.g., temperature, snow and soil moisture data). A more comprehensive design of phenology validation sites is currently being developed by the CEOS-LPV Phenology subgroup, which will provide subsets of remote sensing LSP metrics over PhenoCam sites and bundled with USA-NPN observations. The National Ecological Observatory Network (NEON) is also developing an extensive array of similar phenology relevant observations. Including GPS instruments and the calculation of NMRI time series at these locations would provide critical information to both advance microwave LSP validation and broaden our understanding of vegetation phenology.

References

Dai A, Trenberth KE, Qian T (2004) A global data set of Palmer Drought Severity index for 1870–2002: relationship with soil moisture and effects of surface warming. J Hydrometeorol 5:1117–1130

Estey L, Meertens C (1999) TEQC: the multi-purpose toolkit for GPS/GLONASS data. GPS Solutions 3(1):42–49

Frolking S, Milliman T, McDonald K, Kimball J, Zhao MS, Fahnestock M (2006) Evaluation of the SeaWinds scatterometer for regional monitoring of vegetation phenology. J Geophys Res Atmos 111

Guan K, Wood EF, Caylor KK (2012) Multi-sensor derivation of regional vegetation fractional cover in Africa. Remote Sens Environ 124:653–665

Hansen M, DeFries RS, Townshend JRG, Carroll M, Dimiceli C, Sohlberg RA (2003) Global percent tree cover at a spatial resolution of 500 meters: first results of the MODIS vegetation continuous fields algorithm. Earth Interact 7:1–15

Harris I, Jones PD, Osborn TJ, Lister DH (2013) Updated high-resolution grids of monthly climatic observations—the CRU TS3.10 dataset. Int J Climatol. doi:10.1002/joc.3711

Huffaker CB (1942) Vegetational correlations with vapor pressure deficit and relative humidity. Am Midl Nat 28:486–500

Jackson TJ, Schmugge TJ (1991) Vegetation effects on the microwave emission of soils. Remote Sens Environ 36:203–212

Jones LA, Kimball JS (2011) Daily global land surface parameters derived from AMSR-E. Boulder, Colorado USA: National Snow and Ice Data Center. Digital media (http://nsidc.org/data/nsidc-0451.html)

Jones LA, Kimball JS, McDonald KC, Chan SK, Njoku EG (2009) A method for deriving northern hemisphere vegetation phenology, land surface wetness, and open water fraction from AMSR-E. In: IGARSS Symposium, Cape Town, South Africa

Jones MO, Jones LA, Kimball JS, McDonald KC (2011) Satellite passive microwave remote sensing for monitoring global land surface phenology. Remote Sens Environ 115:1102–1114

Jones MO, Kimball JS, Jones LA, McDonald KC (2012) Satellite passive microwave detection of North America start of season. Remote Sens Environ 123:324–333

Jönsson P, Eklundh L (2004) TIMESAT - a program for analyzing time-series of satellite sensor data. Comput Geosci 30:833–845

Kimball JS, McDonald KC, Running SW, Frolking SE (2004) Satellite radar remote sensing of seasonal growing seasons for boreal and subalpine evergreen forests. Remote Sens Environ 90:243–258

Klein Tank AMG et al (2002) Daily dataset of 20th-century surface air temperature and precipitation series for the European Climate Assessment. Int J Climatol 22:1441–1453

Knowles KW (2004) EASE-grid land cover data resampled from Boston University version of global 1 km land cover from MODIS 2001. In: National Snow and Ice Data Center, Boulder, CO

Knowles KW, Savoie RL, Armstrong RL, Brodzik MJ (2009) AMSR-E/Aqua daily EASE-grid brightness temperatures 2003–2008. In: National Snow and Ice Data Center, Boulder, CO

Larson KM, Small EE (2013) Normalized microwave reflection index, part 1: a vegetation measurement derived from GPS networks. IEEE J Sel Top Appl Earth Obs Remote Sens (in press)

Larson KM, Small EE, Gutmann E, Bilich A, Braun J, Zavorotny V (2008) Use of GPS receivers as a soil moisture network for water cycle studies. Geophys Res Lett 35, L24405

Ma S, Baldocchi D, Xu L, Hehn T (2007) Inter-annual variability in carbon dioxide exchange of an oak/grass savanna and open grass-land in California. Agric For Meteorol 147:157–171

Morisette JT, Richardson AD, Knapp AK et al (2009) Tracking the rhythm of the seasons in the face of global change: phenological research in the 21st century. Front Ecol Environ 7:253–260

Nightingale JM, Morisette JT, Wolfe RE, Tan B, Gao F, Ederer G, Collatz GJ, Turner DP (2009) Temporally smoothed and gap-filled MODIS land products for carbon modeling: application of the fPAR product. Int J Remote Sens 30:1083–1090

Njoku E, Ashcroft P (2005) Global survey and statistics of radio-frequency interference in AMSR-E land observations. IEEE Trans Geosci Remote Sens 43:938–947

Palmer WC (1965) Meteorological drought. Res. Paper no.45. Dept. of Commerce, Washington, DC, 58 pp

Peñuelas J, Rutishauser T, Filella I (2009) Phenology feedbacks on climate change. Science 294:64–65

Piao S, Friedlingstein P, Ciais P, Viovy N, Demarty J (2007) Growing season extension and its impact on terrestrial carbon cycle in the Northern Hemisphere over the past 2 decades. Global Biogeochem Cycles 21:GB3018

Richardson AD, Braswell BH, Hollinger DY, Jenkins JP, Ollinger SV (2009) Near-surface remote sensing of spatial and temporal variation in canopy phenology. Ecol Appl 19:1417–1428

Rienecker MM, Suarez MJ, Gelaro R, Todling R, Bacmeister J, Liu E, Bosilovich MG, Schubert SD, Takacs L, Kim GK, Bloom S, Chen J, Collins D, Conaty A, da Silva A et al (2011) MERRA: NASA's Modern-Era retrospective analysis for research and applications. J Clim 24:3624–3648

Running SW, Nemani RR (1988) Relating seasonal patterns of the AVHRR vegetation index to simulated photosynthesis and transpiration of forests in different climates. Remote Sens Environ 24:347–367

Schwartz MD, Betancourt JL, Weltzin JF (2012) From Caprio's lilacs to the USA national phenology network. Front Ecol Environ 10:324

Shannon CE (1948) A mathematical theory of communication. Bell Syst Techol J 27:379–423, 623–656

Small EE, Larson KM, Braun JJ (2010) Sensing vegetation growth with GPS reflections. Geophys Res Lett 37, L12401

Small EE, Larson KM, Smith W (2013) Normalized microwave reflection index, part 2: validation of vegetation water content estimates at Montana Grasslands. IEEE J Sel Top Appl Earth Obs Remote Sens (in press)

Tan B, Morisette J, Wolfe R (2011) An enhanced TIMESAT algorithm for estimating vegetation phenology metrics from MODIS data. IEEE J Sel Top Appl Earth Obs Remote Sens 4:1–11

Tarpley J, Schneider SR, Money RL (1984) Global vegetation indices from the NOAA-7 meteorological satellite. J Clim Appl Meteorol 23:491–494

Ulaby FT, Moore RK, Fung AK (1981) Microwave remote sensing – active and passive, vol. I: microwave remote sensing fundamentals and radiometry. Artech House, Norwood MA

Van De Griend AA, Wigneron J, Member S (2004) On the measurement of microwave vegetation properties: some guidelines for a protocol. IEEE Trans Geosci Remote Sens 42:2277–2289

White MA, Thornton PE, Running SW, Nemani RR (2000) Parameterization and sensitivity analysis of the BIOME–BGC terrestrial ecosystem model: net primary production controls. Earth Interact 4:1–85

Wolfe DW, Schwartz MD, Lakso AN, Otsuki Y, Pool RM, Shaulis NJ (2005) Climate change and shifts in spring phenology of three horticultural woody perennials in northeastern USA. Int J Biometeorol 49:303–309

Zhang X, Tarpley D, Sullivan JT (2007) Diverse responses of vegetation phenology to a warming climate. Geophys Res Lett 34, L19405